Research Square

Preprints are preliminary reports that have not undergone peer review.
They should not be considered conclusive, used to inform clinical practice,
or referenced by the media as validated information.

Platelet-rich plasma enhances human umbilical cord mesenchymal stem cell-mediated improvement of erectile function and modulates extracellular matrix remodeling in diabetic rats

Jiahao Sun
Xuzhou Medical University
Zhixiang Meng
Southeast University
Pengfei huan
Xuzhou Central Hospital
Wei Wang
Second Hospital of Shandong University
Siyuan Pan
Xuzhou Medical University
Kehan Liu
Xuzhou Medical University
Yu Zhang
Vcanbio Cell & Gene Engineering Corp
Zhilong Dong
Tianjin Cord Blood Bank
Zuobin Zhu
Xuzhou Medical University
Conghui Han
hanconghuidoctor@Vip.qq.com
Xuzhou Medical University

Research Article

Keywords: Diabetic erectile dysfunction, Cavernosal fibrosis, Platelet-rich plasma, Human umbilical cord-derived mesenchymal stem cells, Extracellular matrix remodeling

Posted Date: September 3rd, 2026

DOI: https://doi.org/10.21203/rs.3.rs-10500999/v1

License: This work is licensed under a Creative Commons Attribution 4.0 International License.
Read Full License

Additional Declarations: No competing interests reported.

Platelet-rich plasma enhances human umbilical cord mesenchymal stem cell-mediated improvement of erectile function and modulates extracellular matrix remodeling in diabetic rats

Jiahao Sun[1,3†] ,Zhixiang Meng[2†] , Pengfei Huan[3†] , Wei Wang[4], Siyuan Pan[1], Kehan Liu[1],, Yu Zhang[6], Zhilong Dong[7,] Zuobin Zhu[5*], Conghui Han[1,3*]

[1] Department of Urology, Xuzhou Clinical School of Xuzhou Medical University, Xuzhou 221004, Jiangsu, China.

[2] Urology Department, Xuzhou Central Hospital, School of Medicine, Southeast University, Nanjing 210000, Jiangsu, China.

[3] Xuzhou Central Hospital, Xuzhou 221009, Jiangsu, China.

[4] The Second Hospital of Shandong University, Jinan 250033, Shandong, China.

[5] School of Life Sciences, Xuzhou Medical University, Key Laboratory of Genetic Foundation and Clinical Application, Xuzhou 221004, Jiangsu, China.

[6] VCANBIO Cell & Gene Engineering Corp., ltd., Tianjin, China.

[7] Tianjin Cord Blood Bank, National Industrial Base for Stem Cell Engineering Products, Academic Department, Tianjin, China

[†] **These authors contributed equally to this work.**

[*] **Corresponding authors:**
Conghui Han, E-mail: hanconghuidoctor@vip.qq.com

Zuobin Zhu, E-mail: zhuzuobin@xzhmu.edu.cn

Abstract

Background: Diabetic erectile dysfunction (DMED) involves endothelial injury, smooth muscle dysfunction, cavernosal fibrosis, and disordered extracellular matrix (ECM) remodeling. Mesenchymal stem cells have therapeutic potential but show limited local persistence. Platelet-rich plasma (PRP) contains multiple growth factors, enabling it to provide an optimal microenvironment for mesenchymal stem cells. We investigated whether platelet-

rich plasma (PRP) supports human umbilical cord-derived mesenchymal stem cells (hUC-MSCs), whether concurrent delivery is superior to monotherapy or sequential delivery, and whether benefit is associated with antifibrotic ECM remodeling.

Methods: DMED was induced in male rats with a high-fat diet and streptozotocin. Animals received saline, PRP, hUC-MSCs, sequential hUC-MSCs followed by PRP, or concurrent hUC-MSCs+PRP. Cell viability and colony formation, near-infrared imaging, intracavernous pressure, histology, hydroxyproline, quantitative proteomics, immunofluorescence, and Western blotting were evaluated. Multigroup endpoint data were analyzed using one-way analysis of variance, with one-sample t tests where appropriate; longitudinal body-weight, glucose, and fluorescence curves were analyzed descriptively.

Results: PRP exerted concentration-dependent effects: 10% PRP enhanced hUC-MSC viability and colony formation, whereas 20% PRP was inhibitory. PRP prolonged the local hUC-MSC-associated fluorescence signal. Concurrent hUC-MSCs+PRP improved erectile function more than either monotherapy or sequential treatment and reduced collagen deposition and hydroxyproline. It also restored matrix metalloproteinase 9/Collagen I turnover, increased endothelial nitric oxide synthase and Calponin-1, and improved alpha-smooth muscle actin (α-SMA) abundance on Western blotting and its spatial continuity on immunofluorescence. Proteomics implicated ECM-receptor interaction and the integrin α7-β1 complex. Integrin α7 was higher after concurrent treatment than after hUC-MSCs alone or sequential treatment (both $P < 0.01$). Total Smad2/3 remained stable, whereas treatment reduced the elevated phosphorylated Smad2/3-to-total Smad2/3 ratio and transforming growth factor-β1 expression.

Conclusions: Concurrent PRP and hUC-MSC delivery produced greater benefit than monotherapy or temporally separated treatment. The findings associate improved local MSC activity may be associated with integrin α7-related cell-ECM communication, attenuation of transforming growth factor-β1/Smad profibrotic signaling, normalized matrix turnover, and

improved endothelial and smooth muscle homeostasis. This regimen may offer a rational cell-support strategy for DMED.

Keywords: Diabetic erectile dysfunction; Cavernosal fibrosis; Platelet-rich plasma; Human umbilical cord-derived mesenchymal stem cells; Extracellular matrix remodeling；

1 Introduction

Diabetic erectile dysfunction (DMED) is a common and difficult-to-treat organic complication of diabetes mellitus [1]. Longer diabetes duration, poor metabolic control, and concomitant vascular risk factors further increase the risk of erectile dysfunction (ED) [2]. Persistent hyperglycemia, oxidative stress, and chronic inflammation continuously damage the corpus cavernosum and activate profibrotic responses [1]. Excessive collagen deposition and an imbalance between extracellular matrix (ECM) synthesis and degradation can reduce cavernosal compliance, alter the smooth muscle-to-collagen composition and cell–matrix mechanical coupling, and impair sinusoidal expansion and veno-occlusion, thereby aggravating ED [3]. Studies in diabetic animals have shown that activation of transforming growth factor beta 1 (TGF-β1)/Smad signaling is accompanied by fibromuscular remodeling of the corpus cavernosum, increased collagen and hydroxyproline levels, and impaired erectile function [3]. Abnormal expression of TGF-β1-related fibrotic proteins has also been observed in penile tissue from patients with ED [4]. Cavernosal fibrosis and ECM dysregulation are therefore not merely end-stage histological findings but important pathological processes that translate metabolic injury into hemodynamic dysfunction [5]. Conventional pharmacotherapy primarily improves the short-term hemodynamic response but rarely reverses progressive structural damage; consequently, restoring endothelial, smooth muscle, and ECM homeostasis simultaneously remains a major challenge in the treatment of DMED [6].

Normal penile erection depends on a dynamic balance among the endothelium, smooth muscle, and ECM. Mesenchymal stem cells (MSCs) can promote tissue repair through

paracrine, proangiogenic, anti-inflammatory, and antifibrotic effects [7]. Human umbilical cord-derived mesenchymal stem cells (hUC-MSCs) offer additional advantages, including robust proliferative capacity, low immunogenicity, and a relatively stable source [8]. However, the hyperglycemic, hypoxic, proinflammatory, and profibrotic environment of the diabetic corpus cavernosum accelerates the injury and clearance of transplanted cells [9]. Pharmacokinetic and cell-tracking studies also indicate that long-term persistence of transplanted MSCs in target tissues is generally limited and that detection is influenced by the route of administration, local microenvironment, and tracking method [10] . Stable functional recovery after MSC therapy may therefore require not only preservation of early cell-associated activity after transplantation but also correction of the adverse microenvironment characterized by collagen accumulation, impaired matrix turnover, and disrupted cell–ECM communication.

Platelet-rich plasma (PRP) is prepared from autologous blood by centrifugation and contains numerous growth factors, anti-inflammatory mediators, and matrix-regulatory factors that may provide a transient supportive microenvironment for transplanted MSCs [11]. Randomized controlled trials have suggested that PRP has therapeutic potential for ED, although the evidence of efficacy remains inconsistent[12] . Moreover, growth factor concentrations and PRP composition vary substantially among individuals and preparation methods [13]. PRP and MSCs are considered to have complementary effects in regenerative medicine [14], and in vitro studies have shown that PRP can promote UC-MSC proliferation in a concentration-dependent manner [15]. On this basis, the present study addressed three interrelated questions. First, can PRP at an appropriate concentration improve the biological status of hUC-MSCs and prolong their local retention-related effects in the corpus cavernosum, thereby producing a combined benefit over monotherapy? Second, does the supportive effect of PRP depend on an early temporal window that overlaps with MSC transplantation, such that concurrent administration is superior to temporally separated MSCs→PRP treatment? Third, is

the functional advantage of concurrent treatment accompanied by substantive reversal of cavernosal fibrosis and ECM dysregulation, and how are ITGα7-related cell–ECM communication, MMP9/Collagen I turnover, and TGF-β1/Smad profibrotic signaling molecularly associated with this process?

The ECM is not a passive scaffold. Integrin-mediated bidirectional cell–ECM signaling regulates cell adhesion, survival, cytoskeletal organization, mechanical adaptation, and tissue homeostasis [16]. Integrin α7 (ITGα7) is a muscle-associated integrin subunit that connects smooth muscle cells to the matrix and contributes to vascular smooth muscle homeostasis [17]. In non-penile vascular smooth muscle models, ITGα7 has also been reported to influence TGF-β1 maturation and related signaling; however, this cross-tissue evidence cannot substitute for causal validation in the present study [18]. Meanwhile, Collagen I and MMP9 reflect matrix deposition and degradative turnover [19], whereas TGF-β1/Smad signaling participates in fibroblast activation and profibrotic responses [20]. Integrating these processes within a common framework may help determine whether concurrent treatment restores endothelial and smooth muscle homeostasis by improving cell–matrix communication and ECM turnover.

Against this background, current therapeutic options for DMED remain limited and often provide suboptimal efficacy. Although MSCs and PRP have emerged as promising regenerative therapies for DMED, each has distinct advantages and limitations. It remains unclear whether PRP can enhance the biological activity and local retention of MSCs, whether their concurrent administration is superior to monotherapy or sequential treatment, and through which mechanisms this strategy alleviates cavernosal fibrosis and ECM dysregulation. Therefore, this study aimed to evaluate the supportive effects of PRP on hUC-MSCs, determine the therapeutic advantages of concurrent combination therapy over monotherapy and sequential treatment, and explore the molecular basis underlying its effects on cavernosal fibrosis and ECM dysregulation, thereby providing experimental evidence for regimen optimization and clinical translation of PRP combined with hUC-MSCs for DMED.

2 Materials and methods

2.1 Experimental animals and establishment of the DMED model

A total of 55 six-week-old male Sprague–Dawley rats were obtained from the Laboratory Animal Center of Xuzhou Medical University (Xuzhou, China) and maintained under specific pathogen-free conditions. After a 7-day acclimatization period, five rats continued to receive standard chow as controls, whereas 50 rats received a 60% high-fat diet for 8 weeks for diabetes induction. Based on a previously described model of type 2 diabetes-associated ED [21], high-fat-fed rats were fasted for 12 h and injected intraperitoneally with streptozotocin (STZ; 35 mg/kg). STZ was freshly prepared in 0.1 mol/L citrate buffer (pH 4.5), protected from light, and kept on ice. Rats with a blood glucose concentration >16.7 mmol/L on day 7 were considered diabetic. Apomorphine (APO) screening was performed 2 weeks later. APO was freshly dissolved in saline containing 0.5% vitamin C, protected from light, and administered subcutaneously at 100 μg/kg. Isoflurane anesthesia was used only briefly for APO injection; after full recovery and a 10-min resting period, erectile responses were observed for 60 min. Rats showing no erection were considered to have DMED. No additional inclusion or exclusion criteria were applied.

Of the 50 rats subjected to diabetes induction, six died within 7 days after STZ injection. All 44 surviving rats met the blood glucose criterion for diabetes; 27 met the DMED criterion after APO screening, whereas the remaining 17 were considered unsuccessful models and excluded. Of the 27 eligible DMED rats, 25 were selected using a random-number table and allocated equally, using the same method, to the DMED, PRP, MSCs, MSCs→PRP, and MSCs+PRP groups (n = 5 per group). The remaining two eligible rats were not included. Together with the five control rats, the final groups were Control, DMED, PRP, MSCs, MSCs→PRP, and MSCs+PRP (n = 5 per group). No formal a priori sample-size calculation was performed; group size was determined by the number of animals that successfully met the

DMED criteria. After group allocation, no animals died and no animals, samples, or data points were excluded.

Randomization was performed without stratification or blocking by body weight or blood glucose. Treatment administration, ICP/MAP assessment, and tissue collection were conducted in randomized order. Personnel performing treatment administration, outcome assessment, image and Western blot quantification, proteomic analysis, and statistical analysis were blinded to group allocation; animals and samples were labeled with random identification codes. All animal procedures were approved by the Experimental Animal Ethics Committee of Xuzhou Medical University (approval no. 202503T028). This study was reported in accordance with ARRIVE 2.0. Further details on housing, husbandry, control of potential confounders, anesthesia, welfare monitoring, and humane endpoints are provided in Supplementary Material S2.

2.2 PRP preparation

Autologous whole blood (1 mL) was collected from each rat and mixed with 0.15 mL acid citrate dextrose solution A (ACD-A). The samples were first centrifuged at 400 × g for 10 min; the plasma and buffy coat layers were transferred and then centrifuged at 1500 × g for 15 min. Excess supernatant was discarded, and approximately 200 μL of supernatant was retained to resuspend the platelet pellet, yielding approximately 200 μL of PRP. PRP was activated with chitosan at a final concentration of 175 μg/mL and stored at −20 °C for 15 days before use.

2.3 Culture and characterization of hUC-MSCs

The hUC-MSCs were kindly provided by Vcanbio Cell & Gene Engineering Co., Ltd. (Tianjin, China), and cells from passages 3 to 7 were used. Cells were cultured in low-glucose Dulbecco's modified Eagle medium supplemented with 10% fetal bovine serum and 1% penicillin/streptomycin at 37 °C in 5% CO_2. The MSC phenotype was assessed according to the minimal criteria proposed by the International Society for Cellular Therapy [22]. For flow

cytometry, cells were resuspended in phosphate-buffered saline containing 0.5% bovine serum albumin. The corresponding antibody (2.5 μL) was added to each tube, and the cells were incubated on ice for 30 min in the dark before analysis using a BD Biosciences flow cytometer. Data were analyzed using FlowJo. The antibodies included CD90, CD45, CD73, CD105, CD34, and HLA-DR.Complete antibody information, including suppliers, catalog numbers, and working amounts, is provided in Supplementary Table S1.

2.4 MTT and colony-formation assays

PRP used for the in vitro experiments was prepared using the same procedure as PRP used for animal injection. After activation and storage at −20 °C for 15 days, it was filtered through a 0.22-μm membrane. PRP concentrations of 5%, 10%, and 20% were selected based on previous studies of concentration-dependent MSC responses to PRP [15]. hUC-MSCs were cultured in media containing 10% fetal bovine serum, 0.1% bovine serum albumin, or the indicated PRP concentrations. Cell viability was assessed using the MTT assay after 48 h of PRP exposure, and absorbance was measured at 562 nm. For the colony-formation assay, cells were cultured for 12 days, fixed with paraformaldehyde, stained with 1 mg/mL crystal violet, and counted.

2.5 Grouping and treatment

The PRP group received 200 μL PRP per intracavernous injection. The MSCs group received 1×10^6 hUC-MSCs suspended in 200 μL saline per injection, whereas the MSCs+PRP group concurrently received 1×10^6 hUC-MSCs and 200 μL PRP. The Control and DMED groups received 200 μL saline. These regimens were administered once every 2 weeks for a total of four injections. The sequential MSCs→PRP group first received four MSC injections, followed 1 month later by four PRP injections. For each injection, anesthesia was maintained via a face mask with 2% isoflurane (RWD Life Science Co., Ltd., Shenzhen, China) in oxygen at 400 mL/min, and rats were placed in the supine position. The base of the penis was

temporarily ligated, 200 μL of the corresponding preparation was injected using a 1-mL syringe, and the needle was retained in place for 5 min to facilitate local distribution. Endpoint assessments were performed 2 weeks after the final treatment.

2.6 In vivo imaging

A 5-mM DiR stock solution (MedChemExpress) was prepared in dimethyl sulfoxide, and the working solution was prepared at a 1:1000 dilution. hUC-MSCs were labeled according to established live-cell tracking methods using a lipophilic near-infrared dye. Labeled cells were injected into the corpus cavernosum either alone or concurrently with PRP, with a cell-free control included. Serial imaging was performed every 2 days after injection using an IVIS Lumina S5 in vivo imaging system (CLS148588; excitation/emission = 748/780 nm). The fluorescence-positive area in the penile region was normalized to the first measurement and expressed as the relative fluorescence area (%). Ex vivo imaging of the penis was also performed at the endpoint.

2.7 Assessment of erectile function

Erectile function was assessed 14 days after the final treatment under anesthesia maintained via a face mask with 2% isoflurane in oxygen at 400 mL/min, following established methods for cavernous nerve stimulation and ICP recording in rodents [23]. After exposure of the cavernous nerve, stimulation was applied at 5 V and 15 Hz for 1 min. A pressure needle was inserted into the corpus cavernosum to record ICP, and mean arterial pressure (MAP) was measured by cannulation of the left carotid artery. Three ICP responses were recorded for each animal and averaged. Erectile function was evaluated using ICP and ICP/MAP. Immediately after assessment, rats were placed in an induction chamber and euthanized by continuous exposure to 5% isoflurane until death, after which tissues were collected.

2.8 Histological and immunofluorescence analyses

All paraffin-embedded penile tissue sections were cut at a thickness of 3 μm. Hematoxylin and eosin (H&E) staining and Masson's trichrome staining were used to evaluate cavernosal sinusoidal architecture and collagen/muscle-related tissue composition, respectively. Quantitative analyses were performed at matched anatomical locations using ImageJ [24], with n = 3 per group. Immunofluorescence was performed using a tyramide signal amplification (TSA) double-labeling protocol. After deparaffinization and rehydration, sections underwent antigen retrieval in citrate buffer (pH 6.0). Endogenous enzyme activity was blocked with 3% H_2O_2 for 20 min at room temperature, followed by blocking with 10% goat serum for 30 min at 37 °C. Primary antibodies against eNOS and α-SMA were incubated overnight at 4 °C, followed by horseradish peroxidase (HRP)-conjugated secondary antibodies and TSA detection. Complete primary-antibody information, including suppliers, catalog numbers, and working dilutions, is provided in Supplementary Table S1. eNOS was visualized with TYR-555 and α-SMA with TYR-488, followed by DAPI counterstaining. Fluorescence images were acquired using identical parameters and quantified with ImageJ [24], with n = 3 per group.

2.9 Hydroxyproline assay

Hydroxyproline is a characteristic amino acid highly enriched in collagen, accounting for approximately 13%–14% of collagen dry weight while being present at very low levels in most non-collagenous proteins. Tissue hydroxyproline content is therefore commonly used as an indirect estimate of total collagen burden rather than as a measure of the entire ECM, which also includes proteoglycans and glycoproteins [25]. Mid-cavernosal tissue stored at −80 °C was analyzed using a hydroxyproline assay kit (Nanjing Jiancheng, A030-2-1) according to the manufacturer's instructions, with n = 5 per group. Absorbance was measured at 550 nm using a Synergy2 microplate reader (BioTek, USA), and the results were expressed as μg/mg tissue.

2.10 Proteomic analysis

DIA quantitative proteomic analysis was performed on cavernosal tissues from the Control, DMED, PRP, MSCs, and MSCs+PRP groups, with four biological replicates per group and 20 samples in total. DIA acquisition and quantification followed established methodological principles [26]. Protein identification and annotation were based on the UniProt database (version 2025.02) , and downstream analyses were performed on the Majorbio Cloud platform. Between-group differences were assessed using Student's t test, and differentially expressed proteins were identified using a fold-change threshold of > 1.2 or < 0.83 together with $P < 0.05$. Principal component analysis was used to evaluate global expression patterns. Treatment-rescued proteins were defined as the union of proteins that were upregulated in DMED versus Control and downregulated in Treatment versus DMED, and proteins that were downregulated in DMED versus Control and upregulated in Treatment versus DMED. Gene Ontology (GO) and Kyoto Encyclopedia of Genes and Genomes (KEGG) enrichment analyses were annotated using the corresponding resources . Fisher's exact test was applied, and multiple comparisons were corrected using the Benjamini–Hochberg method; an adjusted P value < 0.05 was considered significantly enriched.

2.11 Western blot analysis

Total protein was extracted from the corpora cavernosa of Sprague–Dawley rats using RIPA lysis buffer (Yamei, PC101) supplemented with enzyme inhibitor (Yamei, GRF101S), and protein concentrations were determined using a BCA protein assay kit (Yamei, ZJ102). Protein samples (30–40 μg per lane) were separated by SDS–PAGE using 10% precast gels (Yamei, PG112) and electrophoresis buffer (Yamei, PS105S), followed by wet transfer to 0.45-μm PVDF membranes (Immobilon-P, IPVH00010). Lablead T3012 transfer buffer was used, and transfer was performed at 300 mA for 45 min. Electrophoresis and transfer were conducted using a PowerPac Basic system (Bio-Rad). Membranes were blocked with rapid protein-free blocking buffer (Yamei, PS108P) for 30 min at room temperature, incubated with primary antibodies for 16 h at 4 °C, and then incubated with secondary antibody for 1 h at room

temperature. Membranes were washed three times for 10 min each with 1× TBST prepared from 10× TBST (Yamei, PS103S). Primary antibodies against Calponin-1, Collagen I, MMP9, p-Smad2/3, α-SMA, total Smad2/3, TGF-β1, ITGα7, and GAPDH were used, together with a goat anti-rabbit secondary antibody. Complete antibody information, including suppliers, catalog numbers, and working dilutions, is provided in Supplementary Table S1. Bands were developed using ECL chemiluminescence reagent (Affinity, KF8003) and captured with a Tanon 4600 chemiluminescence imaging system. Band intensities were analyzed using ImageJ. Target proteins were normalized to GAPDH, and p-Smad2/3 was further normalized to total Smad2/3. Each group included three biological replicates.

2.12 Statistical analysis

All statistical analyses were performed using GraphPad Prism 10.6. ICP and ICP/MAP were prespecified as the primary outcomes. Histological staining, immunofluorescence, hydroxyproline content, and Western blotting were secondary outcomes, whereas proteomic analysis and DiR imaging were exploratory outcomes. Continuous variables were summarized descriptively, and their distributions were assessed using normality and lognormality tests. Multigroup data that met the assumptions of parametric testing were analyzed using ordinary one-way analysis of variance. Where appropriate, one-sample t tests were used to compare values with a prespecified reference value. Longitudinal changes in body weight, blood glucose, and DiR relative fluorescence area were used only to describe temporal trends and were not subjected to inferential statistical testing. Data are presented as the mean ± standard deviation, and $P < 0.05$ was considered statistically significant.

3 Results

3.1 PRP was successfully prepared, hUC-MSC identity was confirmed, and diabetes persisted in the rats

PRP was prepared using a two-step centrifugation protocol and activated with chitosan before use in subsequent experiments (Fig. 1A). Cultured hUC-MSCs exhibited the typical adherent, spindle-shaped, fibroblast-like morphology (Fig. 1B). Flow cytometry showed high expression of CD73, CD90, and CD105 (approximately 99.8%–100%) and minimal expression of CD34, CD45, and HLA-DR (approximately 0.01%–0.04%), consistent with an MSC phenotype (Fig. 1C).

Longitudinal descriptive data showed that body weight increased during the high-fat diet phase and gradually decreased in diabetic animals after STZ injection. Blood glucose rapidly increased and remained high in all diabetic groups (Fig. 1D–F). Local treatment with PRP, MSCs, or the sequential or concurrent combination did not appreciably correct systemic hyperglycemia, suggesting that the subsequent improvement in erectile function predominantly reflected local tissue effects rather than restoration of systemic glucose metabolism.

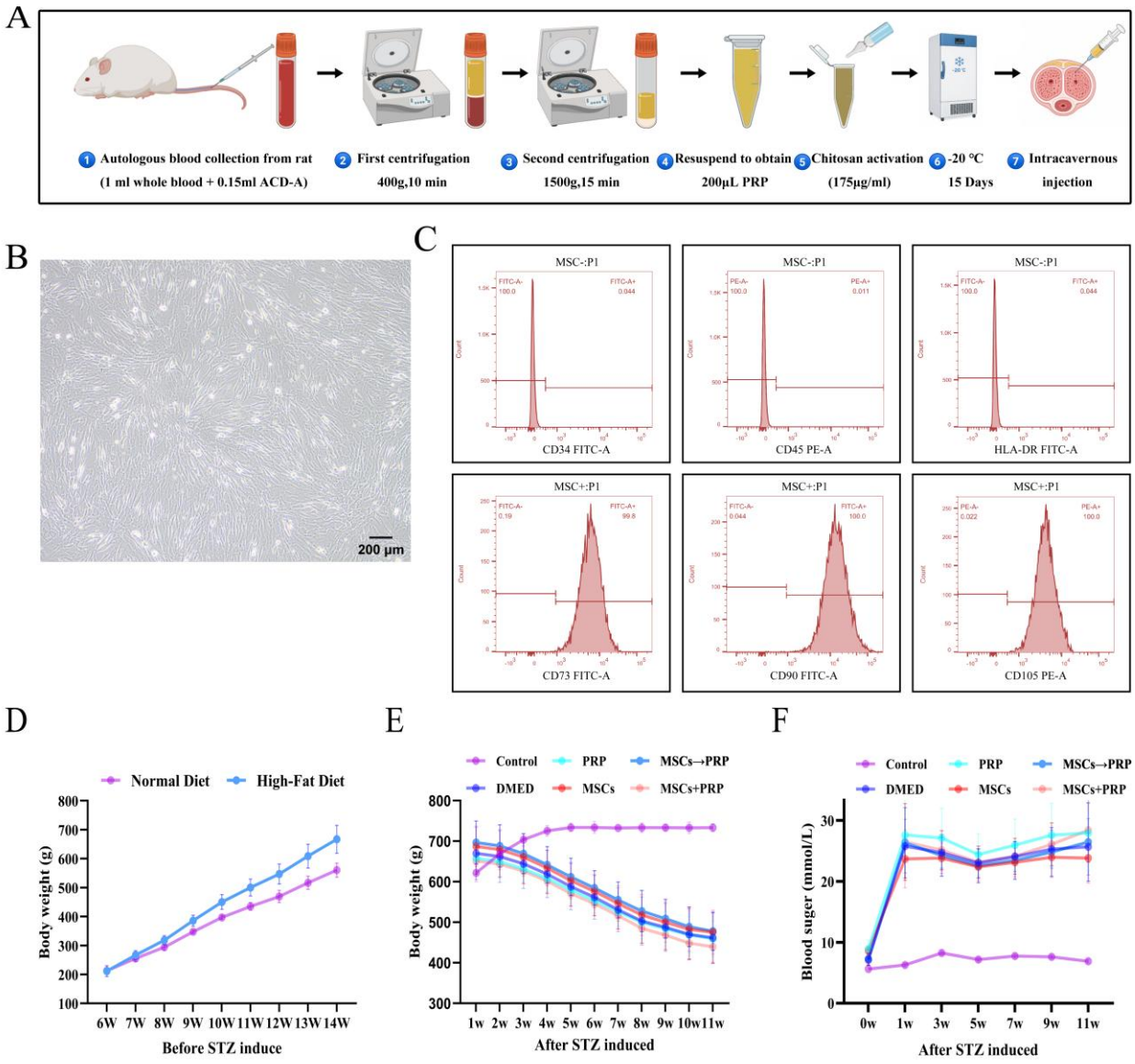


Fig. 1 PRP preparation, hUC-MSC characterization, and the diabetic phenotype

(A) Preparation of autologous rat PRP and intracavernous injection. Whole blood (1 mL) was mixed with 0.15 mL ACD-A. After centrifugation at 400 × g for 10 min, the plasma and buffy coat layers were transferred and centrifuged at 1500 × g for 15 min. Excess supernatant was discarded, and the pellet was resuspended to obtain approximately 200 μL PRP. PRP was activated with 175 μg/mL chitosan and stored at −20 °C for 15 days before use. (B) Representative morphology of hUC-MSCs. (C) Flow cytometric characterization of CD34, CD45, HLA-DR, CD73, CD90, and CD105 expression. (D) Changes in body weight during the high-fat diet phase. (E) Changes in body weight after STZ induction. (F) Changes in blood

glucose after STZ induction. Longitudinal body-weight and blood-glucose curves are presented descriptively and were not subjected to inferential statistical analysis. The illustration in panel A was created using Adobe Illustrator (Adobe Inc., San Jose, CA, USA).

3.2 PRP supports hUC-MSCs within an optimal concentration window, and concurrent treatment produces the greatest functional recovery

The mean absorbance values in the 10% FBS, 0.1% BSA, 5% PRP, 10% PRP, and 20% PRP groups were 1.698, 0.580, 1.117, 1.328, and 0.554, respectively (n = 6). Compared with the nutrient-restricted 0.1% BSA condition, both 5% and 10% PRP increased hUC-MSC viability, with the highest viability among the PRP-treated groups observed at 10% PRP. By contrast, viability in the 20% PRP group decreased to a level close to that in the 0.1% BSA group. The colony-formation assay showed a consistent nonlinear response: colony-forming capacity was greatest with 10% PRP but markedly reduced with 20% PRP (Fig. 2A–C). These findings indicate that PRP support of hUC-MSCs does not increase linearly with concentration but instead occurs within an optimal concentration window.

Compared with the Control group, the DMED group showed marked reductions in ICP and ICP/MAP. PRP, MSCs, and MSCs→PRP each improved the erectile response, whereas the greatest recovery was observed in the concurrent MSCs+PRP group (Fig. 2D–F). Mean ICP values in the Control, DMED, PRP, MSCs, MSCs→PRP, and MSCs+PRP groups were 96.31, 37.46, 72.87, 77.02, 84.49, and 90.03 mmHg, respectively; the corresponding ICP/MAP values were 0.914, 0.362, 0.700, 0.722, 0.784, and 0.849. Concurrent treatment was superior to PRP or MSC monotherapy and to the MSCs→PRP regimen, in which both interventions were administered but separated in time. These findings suggest that coexistence of PRP and MSCs within the same local temporal window may be important for the combined benefit.

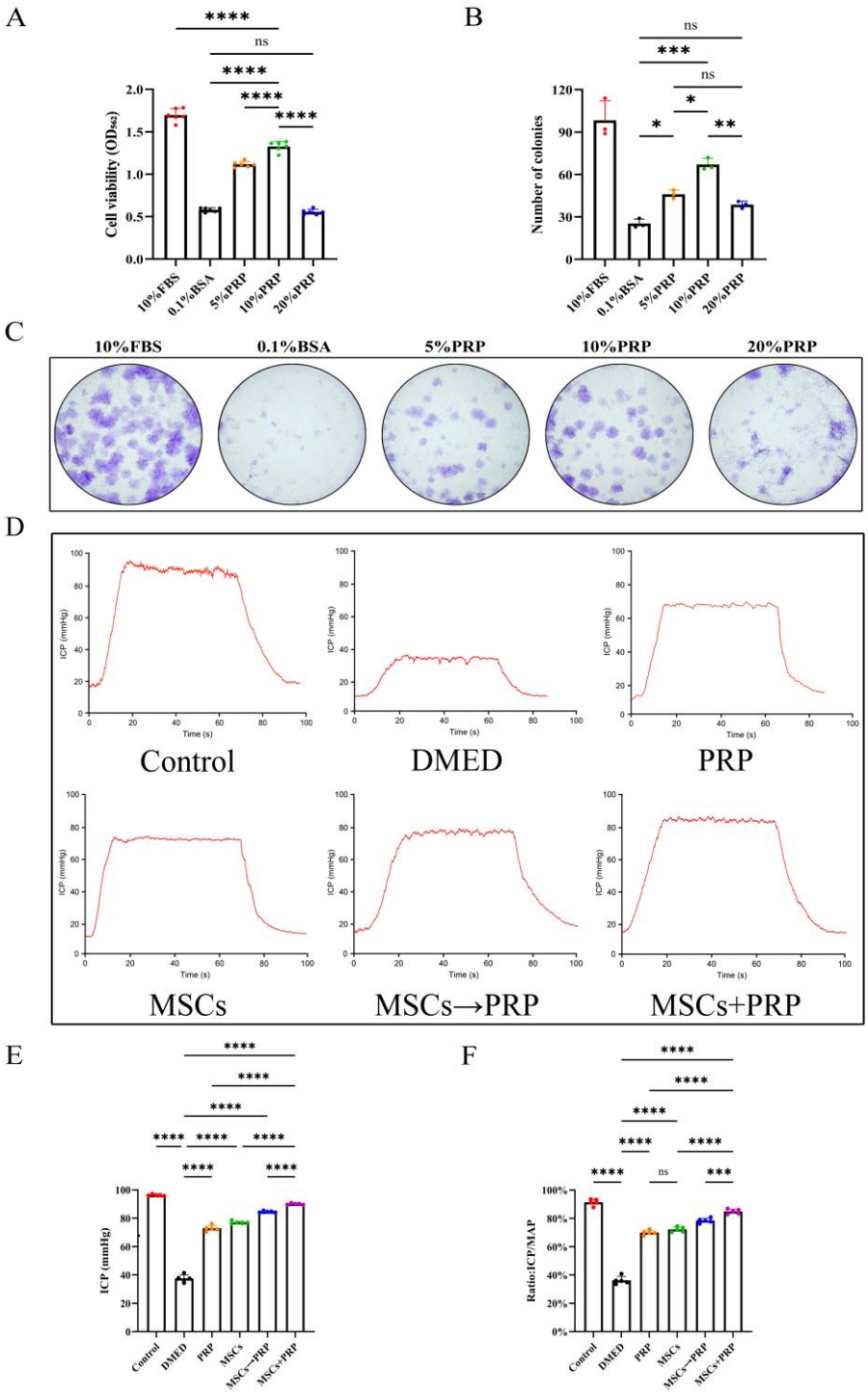


Fig. 2 PRP improves hUC-MSC status, and concurrent MSCs+PRP treatment most effectively restores erectile function

(A) hUC-MSC viability under different culture conditions (n = 6). (B) Quantification of colony numbers (n = 3). (C) Representative images of colony formation. (D) Representative ICP waveforms for each group. (E) Quantification of ICP. (F) Quantification of ICP/MAP. Erectile function was assessed with n = 5 animals per group. Quantitative data are presented as

the mean ± standard deviation. ns, $P \geq 0.05$; *$P < 0.05$; **$P < 0.01$; ***$P < 0.001$; ****$P < 0.0001$.

3.3 PRP prolongs the local MSC-associated fluorescence signal and provides temporal-window evidence for the benefit of concurrent treatment

In vivo imaging showed that the cell-free control remained near background throughout the observation period. Both the MSCs and MSCs+PRP groups exhibited a strong local fluorescence signal at early time points, followed by gradual decay (Fig. 3A). Fluorescence remained detectable through day 12 in all animals in the MSCs group and through day 16 in all animals in the MSCs+PRP group. The relative fluorescence area curves and ex vivo images both showed a more persistent local MSC-associated signal in the combined-treatment group (Fig. 3B, C). The time course was displayed descriptively and was not subjected to inferential statistical testing. Although the DiR signal cannot be equated with the number of viable cells, its direction was consistent with the superior functional outcome in the concurrent-treatment group and supports the possibility that PRP prolongs the local window of MSC-associated activity.

H&E staining showed reduced cavernosal sinusoidal spaces and disorganized tissue architecture in the DMED group. Partial recovery was observed after PRP or MSC treatment, with the most favorable trend in the MSCs+PRP group (Fig. 3D, E). However, some between-treatment differences did not reach statistical significance; this finding therefore supports a favorable structural trend but does not independently establish the absolute superiority of the combined treatment.

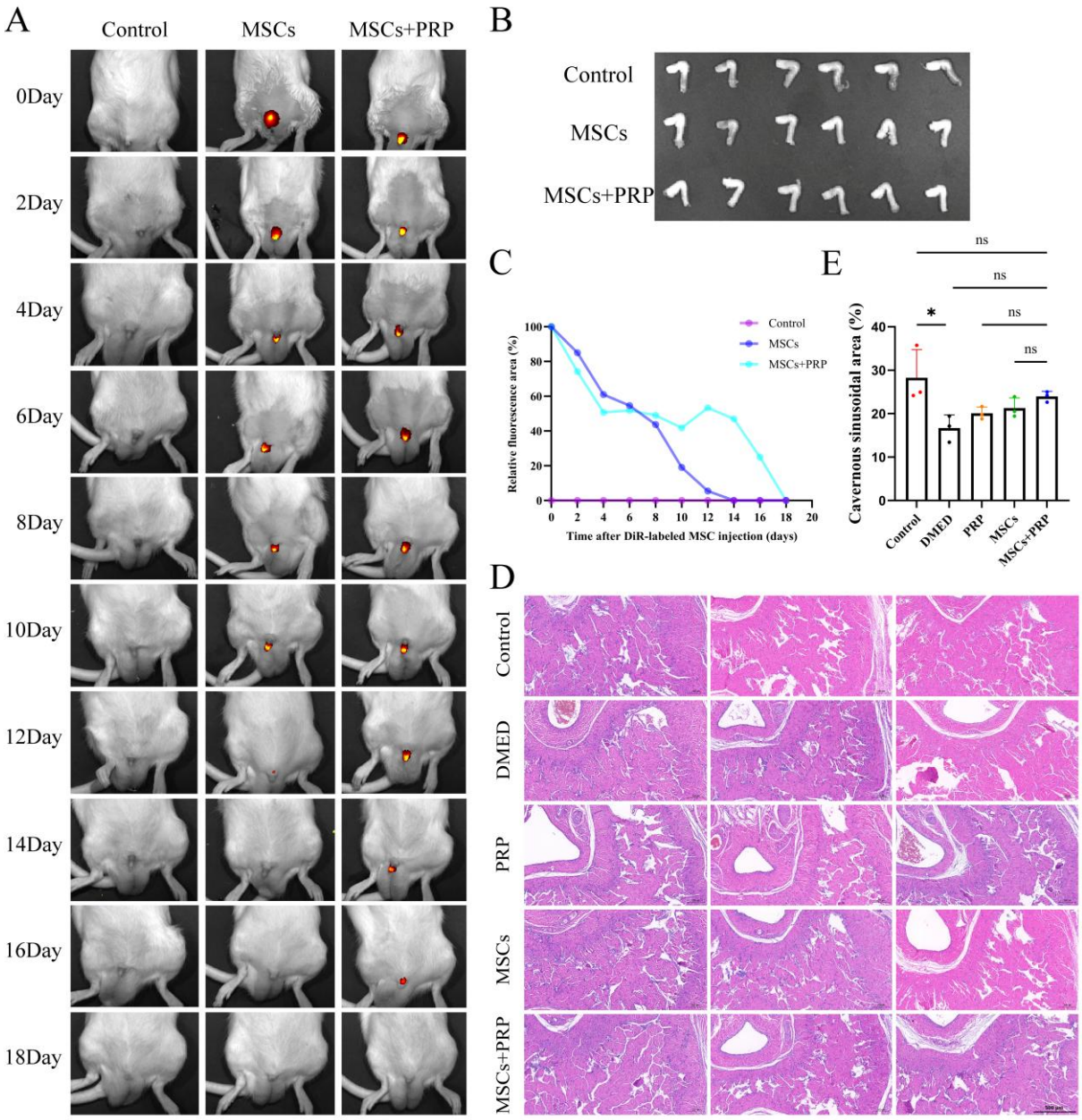


Fig. 3 PRP prolongs the local MSC-associated fluorescence signal and improves the trend in cavernosal sinusoidal architecture

(A) Serial in vivo imaging after injection of DiR-labeled MSCs alone or together with PRP (n = 6). (B) Ex vivo fluorescence images of the penis. (C) Time course of the relative fluorescence area; this curve was analyzed descriptively only. (D) Representative H&E-stained sections from each group. (E) Quantification of the cavernosal sinusoidal space area (n = 3). Data in E are presented as the mean ± standard deviation. ns, $P \geq 0.05$; *$P < 0.05$.

3.4 Concurrent treatment reverses cavernosal fibrosis and dysregulated ECM turnover and improves smooth muscle and endothelial status

To determine whether functional recovery was accompanied by reversal of cavernosal fibrosis, we first evaluated collagen burden and tissue composition. Masson's trichrome staining showed an increased collagen fiber area fraction and a reduced muscle fiber area fraction in the DMED group. PRP and MSCs each produced partial improvement, whereas MSCs+PRP most effectively corrected collagen accumulation and the abnormal muscle-to-collagen composition (Fig. 4A, B). The hydroxyproline assay yielded consistent findings: hydroxyproline content was markedly elevated in the DMED group, decreased to varying degrees in all treatment groups, and was closest to the Control value in the concurrent MSCs+PRP group (Fig. 4C). Mean hydroxyproline contents in the Control, DMED, PRP, MSCs, MSCs→PRP, and MSCs+PRP groups were 1.819, 4.034, 3.477, 3.157, 2.975, and 2.112 μg/mg tissue, respectively (n = 5). The concordant Masson's trichrome and hydroxyproline findings indicate that concurrent treatment produced the most pronounced improvement in cavernosal fibrosis.

Western blotting showed increased Collagen I and reduced MMP9 expression in the DMED group. After treatment, these proteins changed in opposite directions toward the Control pattern, with the largest changes observed in the concurrent MSCs+PRP group (Fig. 4D–F). Together with the reductions in collagen fiber area and hydroxyproline content, the combination of reduced Collagen I and restored MMP9 supports the interpretation that concurrent treatment attenuates pathological collagen accumulation and promotes normalization of dysregulated ECM turnover rather than simply suppressing all matrix components.

α-SMA immunofluorescence showed reduced signal intensity, sparse spatial distribution, and disrupted continuity in the DMED group. Recovery trends were observed after PRP and MSC treatment, with the greatest improvement in the concurrent MSCs+PRP group (Fig. 4G,

H). Relative α-SMA fluorescence intensity was significantly higher in the MSCs+PRP group than in the DMED group ($P < 0.05$), but did not differ significantly from the Control, PRP, or MSCs groups. Whole-tissue Western blotting showed a concordant directional pattern: the α-SMA/GAPDH ratio was reduced in the DMED group and increased to varying degrees after treatment. The α-SMA/GAPDH ratio in the MSCs+PRP group was significantly higher than those in the DMED ($P < 0.0001$), PRP, MSCs, and MSCs→PRP groups (all $P < 0.05$), but was comparable to that in the Control group ($P \geq 0.05$) (Fig. 4I, J). Calponin-1 expression was reduced in the DMED group and increased after treatment, with the greatest recovery in the concurrent-treatment group (Fig. 4I, K). Taken together, the concordant immunofluorescence and Western blot findings indicate recovery of α-SMA abundance and spatial continuity, while Calponin-1 further supports improvement in the contractile smooth muscle phenotype.

eNOS expression was markedly reduced in the DMED group, partially restored after MSC treatment, and highest in the concurrent MSCs+PRP group. Expression in the concurrent-treatment group was significantly higher than that in the DMED, PRP, and MSCs groups and did not differ significantly from the Control group (Fig. 4L, M). These findings indicate that concurrent treatment substantially improves cavernosal endothelial status.

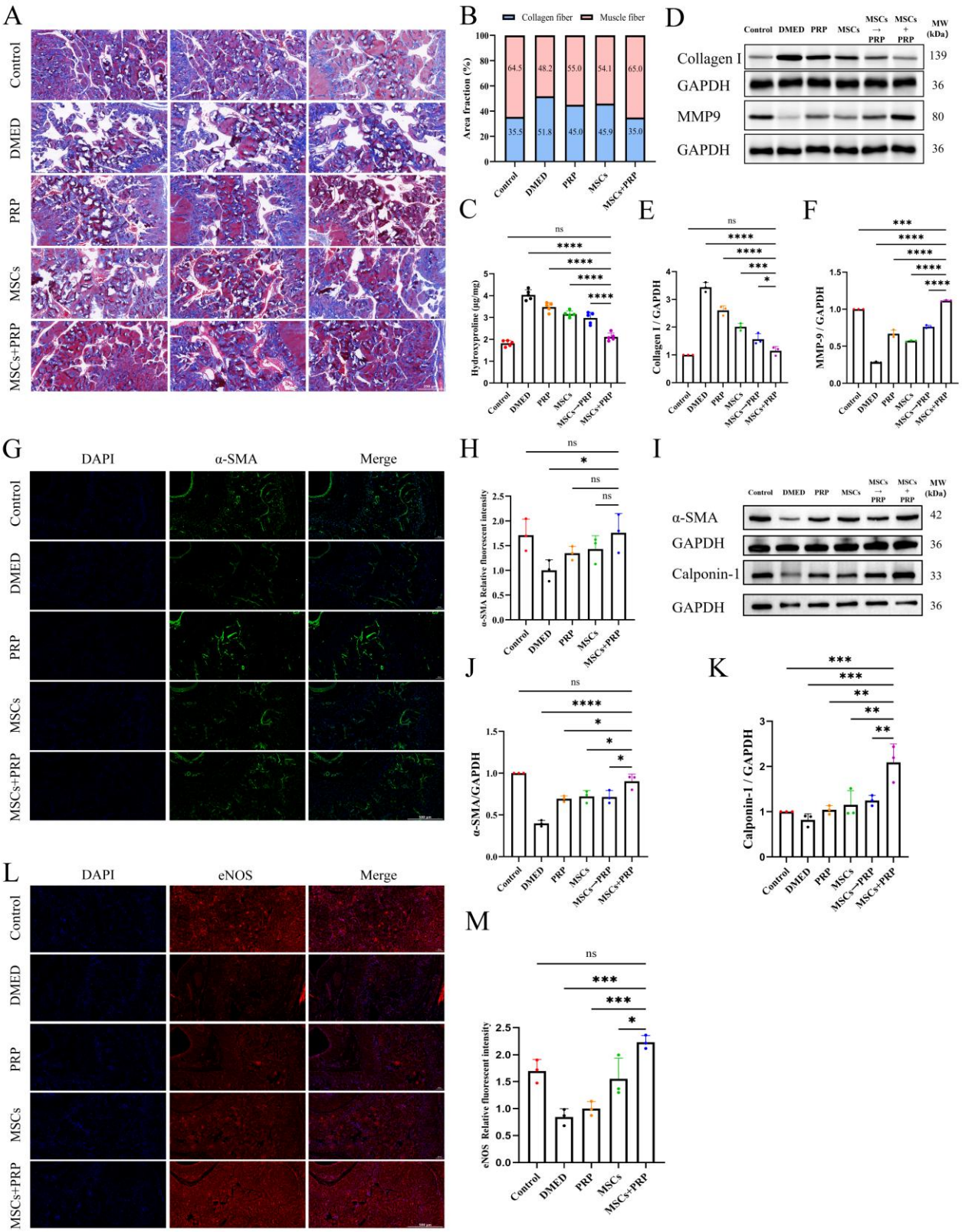


Fig. 4 Concurrent MSCs+PRP treatment attenuates cavernosal fibrosis and improves ECM turnover and smooth muscle and endothelial status

(A) Masson's trichrome staining of rat corpus cavernosum. (B) Area fractions of collagen fibers and muscle fibers (n = 3). (C) Hydroxyproline content in each group (μg/mg tissue, n =

5). (D) Representative Western blots of Collagen I, MMP9, and GAPDH. (E) Densitometric quantification of Collagen I. (F) Densitometric quantification of MMP9. (G) α-SMA immunofluorescence. (H) Relative α-SMA fluorescence intensity (n = 3). (I) Representative Western blots of α-SMA, Calponin-1, and GAPDH. (J) Densitometric quantification of α-SMA. (K) Densitometric quantification of Calponin-1. (L) eNOS immunofluorescence. (M) Relative eNOS fluorescence intensity (n = 3). Western blotting included n = 3 biological replicates per group. Quantitative data are presented as the mean ± standard deviation. ns, $P \geq 0.05$; *$P < 0.05$; **$P < 0.01$; ***$P < 0.001$; ****$P < 0.0001$.Blots were cropped for presentation. Full-length blots/gels are presented in Supplementary Figure S3.

3.5 Proteomics implicates ECM–receptor interaction and the integrin α7–β1 complex as candidate mechanisms

DIA proteomics was performed on 20 samples and identified 9,227 proteins and 102,460 peptides. Volcano plots revealed extensive expression changes between the DMED and Control groups and distinct protein response patterns after PRP, MSCs, and MSCs+PRP treatment (Fig. 5A).

Venn analysis of treatment-rescued proteins identified 15 proteins shared by all three treatments. The MSCs+PRP, MSCs, and PRP groups had 54, 74, and 39 treatment-specific rescued proteins, respectively, together with varying pairwise overlaps (Fig. 5B). Principal component analysis and heat-map analysis further showed differences in the global protein expression profiles among groups (Fig. 5C, D). In the KEGG analysis, ECM–receptor interaction did not meet the significance threshold after Benjamini–Hochberg correction; nevertheless, it was selected as a candidate pathway for subsequent validation based on its ranking, the composition of the rescued proteins, and the structural pathology of DMED (Fig. 5E). GO enrichment analysis displayed relevant terms across biological process, cellular

component, and molecular function categories. Within the cellular component category, the integrin α7–β1 complex was directionally consistent with the ECM–receptor axis (Fig. 5F), although this term also failed to reach the adjusted significance threshold. ITGα7 was primarily detected in treatment-rescued sets that included MSCs and was absent from the PRP-only rescued set. Thus, the proteomic findings do not directly demonstrate pathway activation but nominate ITGα7-related cell–ECM communication for subsequent validation.

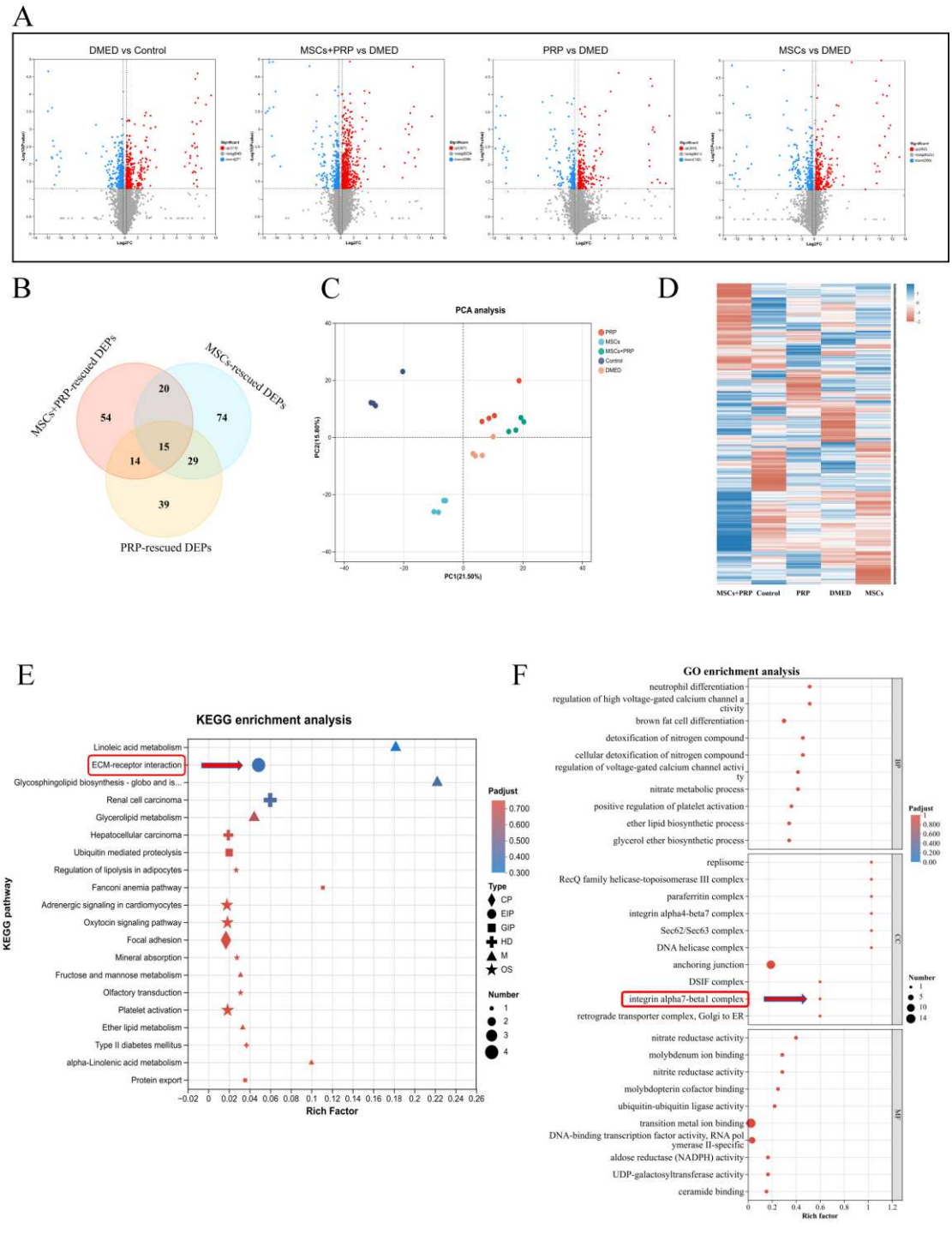


Fig. 5 Proteomics identifies treatment-rescued proteins and implicates ECM–receptor/ITGα7-related remodeling

(A) Volcano plots of differentially expressed proteins for DMED versus Control, MSCs+PRP versus DMED, PRP versus DMED, and MSCs versus DMED. (B) Venn diagram of proteins rescued by PRP, MSCs, and MSCs+PRP treatment. (C) Principal component analysis. (D) Hierarchical clustering heat map. (E) KEGG enrichment analysis, with ECM–receptor interaction boxed. (F) GO enrichment analysis showing biological process (BP), cellular component (CC), and molecular function (MF) categories, with the integrin α7–β1 complex boxed. Color indicates the adjusted P value, and bubble size indicates the number of proteins within each term. The boxed terms did not meet the adjusted significance threshold and are presented only as candidate mechanistic clues.

3.6 Concurrent treatment coordinates ITGα7-related cell–ECM communication and TGF-β1/Smad signaling to remodel the pathological ECM

ITGα7 expression was markedly reduced in DMED tissue, showed limited recovery after PRP monotherapy, and recovered to varying degrees in treatment groups that included MSCs (Fig. 6A, B). Notably, ITGα7 expression in the concurrent MSCs+PRP group was significantly higher than that in both the MSCs and MSCs→PRP groups (both $P < 0.01$), indicating that coexistence of PRP and MSCs within the same local temporal window was closely associated with stronger ITGα7 recovery. This finding is directionally consistent with the proteomic signals for ECM–receptor interaction and the integrin α7–β1 complex, but remains correlative and does not establish ITGα7 as a direct causal target of PRP.

TGF-β1 and p-Smad2/3 expression was increased in the DMED group and decreased to varying degrees after treatment, with the largest reduction in the concurrent-treatment group (Fig. 6A, C, D). Total Smad2/3 remained broadly stable across groups (Fig. 6A, E), whereas

the p-Smad2/3/Smad2/3 ratio was elevated in the DMED group, decreased after treatment, and was lowest in the concurrent-treatment group (Fig. 6F). The stability of total Smad2/3 indicates that the change in this ratio predominantly reflects altered Smad2/3 phosphorylation rather than fluctuations in total protein abundance. Together with the coordinated changes in Collagen I, hydroxyproline, and Masson's trichrome staining shown in Fig. 4, these findings support attenuation of TGF-β1/Smad-related profibrotic signaling by concurrent treatment.

Integrating the findings from Figs. 4–6, we propose the following interpretive sequence. In DMED, increased collagen deposition, reduced MMP9, and aberrant activation of TGF-β1/Smad2/3 collectively promote defective ECM turnover and cavernosal fibrosis, accompanied by reduced ITGα7 and impaired cell–matrix connections. By improving the early persistence of local MSC-associated activity, concurrent MSCs+PRP treatment may simultaneously enhance ITGα7-related adhesion/communication and attenuate TGF-β1/Smad profibrotic signaling. These two lines of evidence converge on reduced Collagen I and hydroxyproline, restoration of MMP9, and subsequent ECM remodeling, together with improvements in Calponin-1, α-SMA expression and spatial continuity, eNOS, ICP, and ICP/MAP. Figure 6G presents this integrated mechanistic model; crosstalk between ITGα7 and TGF-β1/Smad remains a hypothesis requiring further validation.

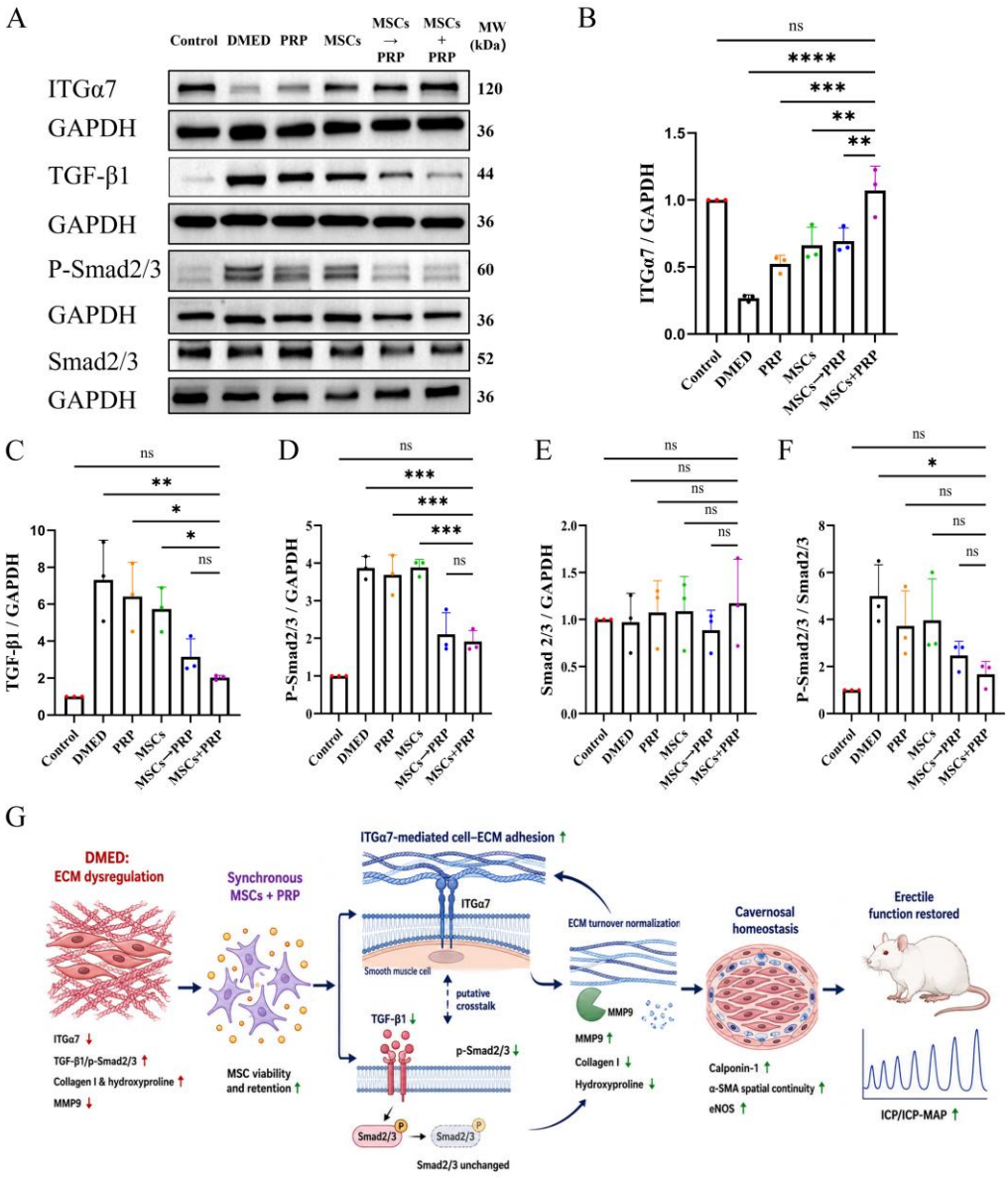


Fig. 6 Concurrent MSCs+PRP treatment coordinates ITGα7-related cell–ECM communication and TGF-β1/Smad signaling and remodels the pathological ECM

(A) Representative Western blots of ITGα7, TGF-β1, p-Smad2/3, Smad2/3, and GAPDH. (B) Densitometric quantification of ITGα7. (C) Densitometric quantification of TGF-β1. (D) Densitometric quantification of p-Smad2/3. (E) Densitometric quantification of total Smad2/3. (F) p-Smad2/3/Smad2/3 ratio. (G) Integrated mechanistic model based on the present findings. DMED-associated ECM dysregulation is characterized by reduced ITGα7, increased TGF-β1/p-Smad2/3, increased Collagen I and hydroxyproline, and reduced MMP9. By prolonging local MSC-associated activity, concurrent MSCs+PRP treatment enhances ITGα7-mediated

cell–ECM adhesion/communication and attenuates TGF-β1/Smad profibrotic signaling, thereby restoring ECM turnover, improving cavernosal homeostasis, and increasing ICP and ICP/MAP. Solid lines denote associations supported by the present findings, whereas dashed lines indicate potential crosstalk that requires causal validation. Western blotting included n = 3 biological replicates per group. Quantitative data are presented as the mean ± standard deviation. ns, $P \geq 0.05$; *$P < 0.05$; **$P < 0.01$; ***$P < 0.001$; ****$P < 0.0001$. Blots were cropped for presentation. Full-length blots/gels are presented in Supplementary Figure S3. The illustration in panel G was created using Adobe Illustrator (Adobe Inc., San Jose, CA, USA).

4 Discussion

The present study addressed the three questions posed in the Introduction through a sequential evidence chain encompassing cellular support and persistence of local activity, comparison of concurrent and sequential administration, and fibrosis/ECM remodeling and their molecular associations. The principal findings were as follows: PRP at an appropriate concentration improved hUC-MSC status and prolonged the local MSC-associated signal; concurrent MSCs+PRP treatment improved ICP and ICP/MAP more effectively than temporally separated MSCs→PRP treatment; and this advantage was accompanied by attenuated cavernosal fibrosis, restoration of MMP9/Collagen I-related ECM turnover, enhanced ITGα7-related cell–ECM connectivity, reduced TGF-β1/Smad profibrotic signaling, and improved endothelial and smooth muscle status. These findings support an integrated framework in which improved early local MSC-associated activity may coordinate cell–ECM communication and profibrotic signaling, remodels the pathological ECM, and restores cavernosal homeostasis and erectile function.

This study employed a stepwise experimental approach comprising in vitro dose screening, colony formation validation, in vivo imaging, and functional comparisons to investigate the

effects of PRP on MSC status and retention. The diabetic corpus cavernosum is persistently exposed to hyperglycemia, oxidative stress, and a proinflammatory and profibrotic milieu, leading to rapid attenuation of cell-associated activity after transplantation [1, 9]. In the present study, concurrent PRP administration prolonged the local DiR-associated signal, consistent with the cell-viability and colony-formation findings and with the superior functional outcome of concurrent treatment. Therefore, we propose that PRP may create a transient supportive microenvironment, improve MSC status, and prolong the persistence of MSC-related signals or paracrine activity within the target tissue. Studies in other tissue-repair settings have similarly shown that PRP-derived exosomes enhance MSC activity and reparative effects, providing indirect support for this interpretation [27].

At the dose level, the effect of PRP on hUC-MSCs was clearly nonlinear. Both 5% and 10% PRP increased cell viability at 48 h, with 10% PRP producing the best response among the PRP-treated conditions, whereas 20% PRP conferred no further benefit and instead reduced cell viability and colony formation. Previous studies have likewise demonstrated concentration-dependent effects of PRP on MSCs, although the optimal concentration varies with the PRP preparation method, cell source, and experimental conditions [15]. Meta-analyses of randomized clinical studies have not reached fully consistent conclusions regarding the magnitude and durability of benefit from PRP monotherapy for ED [28], potentially in part because of heterogeneity in PRP composition and growth factor concentrations [13]. Thus, our findings provide phenotypic evidence that PRP, within an appropriate concentration range, supports hUC-MSCs and that concurrent combination therapy yields superior functional outcomes.

In this study, we compared monotherapies, sequential MSCs→PRP therapy, and concurrent MSCs+PRP combination therapy.The sequential group received both MSCs and PRP but with temporal separation, whereas the concurrent group exposed MSCs and PRP to the same local microenvironment during the early post-transplantation period. Studies of MSC

kinetics in vivo have shown that the distribution, clearance, and short-term persistence of transplanted cells are strongly time-dependent [10]. The higher ICP and ICP/MAP, more persistent DiR-associated signal, and stronger ITGα7 recovery in the concurrent group collectively support the possibility that the principal supportive value of PRP occurs early after MSC transplantation and amplifies local reparative effects by overlapping with the MSC activity window. Recent findings in other tissue models, in which PRP promoted integrin β1-related homing of UC-MSCs and a platelet-rich fibrin shield enhanced MSC survival, provide indirect support for this early coexistence microenvironment [29]. Thus, the study demonstrates an efficacy difference between the two prespecified administration regimens and supports the temporal-overlap interpretation.

Previous studies of DMED have shown that hUC-MSCs improve erectile function and modulate TGF-β-, α-SMA-, and collagen-related changes [30], whereas PRP has also shown some protective effect on erectile function in STZ-induced diabetic rats [31]. Hydroxyproline accounts for approximately 13%–14% of collagen dry weight and can serve as a surrogate for total tissue collagen burden, but it does not represent all ECM components, such as proteoglycans and glycoproteins [25]. In the present study, DMED increased Masson's trichrome-positive collagen and hydroxyproline content, upregulated Collagen I, and reduced MMP9, whereas concurrent treatment produced the strongest reversal across these endpoints. Previous work has linked MMP-related degradative activity in the corpus cavernosum to antifibrotic remodeling and erection-associated signaling [32]. These findings indicate that DMED is not simply a state of “excess ECM” but instead involves the coexistence of pathological collagen accumulation and impaired physiological matrix turnover; concurrent treatment appears to restore ECM homeostasis. Because sinusoidal expansion and veno-occlusion depend on tissue compliance and an appropriate smooth muscle-to-collagen composition, these changes provide a structural explanation for recovery of ICP and ICP/MAP.

Moreover, proteomic analysis revealed that the three treatments shared a core set of treatment-rescued proteins while also eliciting treatment-specific responses. Concurrent treatment yielded 54 treatment-specific rescued proteins, indicating that its protein expression pattern was not a complete overlap of the responses to the individual treatments. Changes in ECM composition and mechanical properties can feed back to regulate cell behavior, providing strong biological plausibility for ECM–receptor interaction [16, 19]. Although neither ECM–receptor interaction nor the integrin α7–β1 complex reached the enrichment threshold after multiple-testing correction, they converged on cell–ECM communication at the pathway and cellular-component levels and were directionally consistent with subsequent ITGα7 validation. These enrichment results therefore fulfilled their role in nominating a candidate network but cannot independently demonstrate pathway activation.

The ITGα7 validation findings further strengthened this mechanistic chain. ITGα7 expression in the concurrent MSCs+PRP group was not only higher than that in the DMED and PRP groups but also significantly elevated relative to the MSCs and MSCs→PRP groups (both $P < 0.01$). Thus, the restoration of ITGα7 cannot be explained solely by MSC treatment alone and is tightly associated with simultaneous PRP and MSC activity within the same local therapeutic window. As an integrin subunit anchoring smooth muscle cells to the ECM, ITGα7 maintains smooth muscle homeostasis and has been linked to the modulation of TGF-β1 signaling in other vascular models [17, 18]. In addition, recent evidence showing that PRP boosts integrin β1-mediated homing of UC-MSCs implies PRP modulate integrin-dependent cell–matrix crosstalk, though such cross-tissue evidence only provides indirect support [29]. ITGα7 may help restore smooth muscle–matrix adhesion and mechanical homeostasis, thereby linking MSC-associated repair to ECM remodeling. Collectively, the convergence of proteomic nomination, exclusive ITGα7 upregulation observed under the concurrent regimen, and its established biological functions positions this integrin as a compelling mechanistic hub connecting improved cell–ECM adhesion to downstream antifibrotic remodeling. While direct

causal perturbation assays targeting ITGα7 lie beyond the scope of this regimen-comparison study, the coordinated upregulation of ITGα7, accompanied by suppressed TGF-β1/Smad profibrotic signaling and normalized MMP9/Collagen I turnover, supports an integrated working model: PRP-sustained MSC viability re-establishes physiological cell–ECM communication, which further propagates tissue-reparative signaling cascades. Definitive dissection of ITGα7-centered causal effects—including its potential crosstalk with TGF-β1 activation—remains a prioritized direction for follow-up mechanistic investigations.

Previous studies in diabetic animals have shown that TGF-β1/Smad activation is accompanied by increased penile collagen, fibronectin, and hydroxyproline and by impaired erectile function [3]. More recent interventions targeting Smad signaling or the TSP1–TGF-β axis have similarly attenuated cavernosal fibrosis and improved erectile function in diabetic rats [33]. In the present study, total Smad2/3 remained broadly stable across groups, whereas the p-Smad2/3/Smad2/3 ratio was elevated in the DMED group and decreased after treatment, in parallel with reductions in TGF-β1, Collagen I, and hydroxyproline and restoration of MMP9. Concurrent treatment therefore appears more likely to attenuate TGF-β1/Smad-related profibrotic signaling by suppressing aberrant Smad2/3 phosphorylation than by reducing total Smad2/3 expression.

The endothelial and smooth muscle findings further link the molecular changes to functional recovery. Previous studies of DMED have shown that disruption of the Akt/Hsp90β/eNOS complex and NOX-related oxidative stress impair eNOS function, whereas restoration of eNOS contributes to an improved erectile response [34, 35]. In the present study, eNOS expression was reduced in DMED and substantially restored by concurrent treatment, providing a physiological basis for the improvement in ICP. Calponin-1 was reduced in the DMED group and showed the greatest recovery after concurrent treatment, supporting improvement in the contractile smooth muscle phenotype. Senescence and phenotypic alterations of cavernosal smooth muscle cells have also been implicated in aggravating fibrosis

and ED [36]. Importantly, α-SMA immunofluorescence and whole-tissue Western blotting showed concordant directional changes. Immunofluorescence demonstrated reduced signal and disrupted spatial continuity in DMED and improvement after concurrent treatment, whereas Western blotting showed a lower α-SMA/GAPDH ratio in DMED and a treatment-associated recovery. The concurrent group had a significantly higher ratio than the DMED, PRP, MSCs, and MSCs→PRP groups, while remaining statistically comparable to the Control group. Together with the pronounced increase in Calponin-1, these findings support improvement in both smooth muscle structural continuity and the contractile phenotype. Single-cell studies indicate that multiple cell types in the diabetic corpus cavernosum undergo heterogeneous changes [37] therefore, α-SMA should still be interpreted alongside Calponin-1, Masson's trichrome staining, eNOS, and functional measures rather than as an isolated measure of smooth muscle recovery.

From a translational perspective, systematic reviews of stem cell therapy for DMED generally support preclinical benefit [38], but the MSC secretome remains a candidate strategy [39], and current human studies and trials combining MSCs with physical modalities have largely been small or exploratory [40]. Taken together, this study established a relatively comprehensive association-based mechanistic framework. In vitro, cell-tracking, and functional evidence indicated that PRP at an appropriate concentration could support hUC-MSC status and prolong local MSC-related signals. Functional and molecular findings further demonstrated that concurrent combination therapy was superior to the predefined sequential regimen. Finally, multiple indicators collectively confirmed corpus cavernosum fibrosis and ECM dysregulation, whose amelioration was coherently associated with restored ITGα7 expression, attenuated TGF-β1/Smad signaling, and functional recovery.

This study also has several limitations. First, DiR is a lipophilic in vivo tracer, and its fluorescence cannot reliably distinguish viable transplanted cells from residual dye or dye transfer. Therefore, the findings of this study should be interpreted in light of MSC kinetics and

the inherent limitations of the tracking method [10]. Second, the treatment duration and endpoint timing of the sequential group were not fully matched to those of the concurrent combination group, and the sequential group was not included in the complete histological and proteomic analyses. Finally, this study lacked ITGα7-targeted interventions and other experiments required for causal validation. Nevertheless, the available evidence supports the protocol-level advantage of concurrent combination therapy and an association-based mechanistic model involving antifibrotic effects and ECM remodeling.

5 Conclusions

Concurrent intracavernous administration of PRP and hUC-MSCs improved erectile function in rats with DMED more effectively than PRP, MSCs, or temporally separated sequential MSCs→PRP treatment. This benefit may be associated with PRP-mediated improvement of hUC-MSC status and prolongation of local MSC-associated activity, enhanced ITGα7-related cell–ECM communication, attenuation of TGF-β1/Smad2/3 profibrotic signaling, restoration of MMP9/Collagen I-related turnover, and reductions in collagen and hydroxyproline burden. Together, these changes promoted remodeling of the pathological ECM and were accompanied by recovery of smooth muscle and endothelial status and erectile function. The present study provides relatively comprehensive phenotypic and regimen-comparison evidence for PRP-mediated support and the advantage of concurrent administration and establishes a multilevel associative mechanism involving fibrosis and ECM remodeling. However, synergy in the strict sense, pure temporal causality, ITGα7–TGF-β1/Smad crosstalk, and the independent contribution of ECM remodeling to functional recovery require further validation.Future studies should focus on elucidating the specific mechanisms by which PRP supports hUC-MSCs and further validate the causal role of ITGα7 in regulating ECM remodeling through targeted interventions. Meanwhile, studies with larger sample sizes are needed to optimize the dosage and administration regimen of the combination therapy and

systematically evaluate its long-term efficacy and safety, thereby providing a basis for clinical translation.

List of abbreviations

ACD-A, acid citrate dextrose solution A; Akt, protein kinase B; BCA, bicinchoninic acid; BSA, bovine serum albumin; DAPI, 4′,6-diamidino-2-phenylindole; DIA, data-independent acquisition; DiR, 1,1′-dioctadecyl-3,3,3′,3′-tetramethylindotricarbocyanine iodide; DMED, diabetic erectile dysfunction; ECM, extracellular matrix; ECL, enhanced chemiluminescence; ED, erectile dysfunction; eNOS, endothelial nitric oxide synthase; FBS, fetal bovine serum; GAPDH, glyceraldehyde-3-phosphate dehydrogenase; GO, Gene Ontology; H&E, hematoxylin and eosin; HLA-DR, human leukocyte antigen-DR; HRP, horseradish peroxidase; Hsp90β, heat shock protein 90 beta; hUC-MSCs, human umbilical cord-derived mesenchymal stem cells; ICP, intracavernous pressure; ITGα7, integrin alpha 7; IVIS, in vivo imaging system; KEGG, Kyoto Encyclopedia of Genes and Genomes; MAP, mean arterial pressure; MMP9, matrix metalloproteinase 9; MSCs, mesenchymal stem cells; MTT, 3-(4,5-dimethylthiazol-2-yl)-2,5-diphenyltetrazolium bromide; NOX, NADPH oxidase; PBS, phosphate-buffered saline; PRP, platelet-rich plasma; p-Smad2/3, phosphorylated Smad2/3; PVDF, polyvinylidene fluoride; RIPA, radioimmunoprecipitation assay; SDS–PAGE, sodium dodecyl sulfate–polyacrylamide gel electrophoresis; STZ, streptozotocin; TBST, Tris-buffered saline containing Tween 20; TGF-β1, transforming growth factor beta 1; TSA, tyramide signal amplification; TSP1, thrombospondin 1; α-SMA, alpha-smooth muscle actin.

Declarations

Ethics approval and consent to participate

The animal study was approved by the Experimental Animal Ethics Committee of Xuzhou Medical University (approval no. 202503T028). All procedures were conducted in accordance with institutional guidelines for the care and use of laboratory animals.

Approved project title:Exploring the feasibility of combined therapy using enriched platelet plasma and stem cells for diabetic erectile dysfunction; approval date: March 8, 2025

The hUC-MSCs used in this study were provided by Vcanbio Cell & Gene Engineering Co., Ltd. (Tianjin, China) and were derived from donated human umbilical cord tissue obtained with the donor's written informed consent. The provision and use of the hUC-MSCs were conducted under the ethical approval for the clinical research collaboration between Vcanbio and Xuzhou Central Hospital. All donor information was de-identified and kept strictly confidential.

Consent for publication

Not applicable.

Availability of data and materials

The datasets used and/or analyzed during the current study are available from the corresponding author on reasonable request.

Competing interests

The authors declare that they have no competing interests.

Funding

This research was supported by New Round of Xuzhou " Pengcheng Talent Program" - High-level Healthcare Talent Recruitment and Development Project (Project Number: 2-2025DF06）; The China Postdoctoral Science Foundation(Certificate Number: 2024M752699); and Jiangsu Funding Program for ExcellentPostdoctoral Talent. The funders had no role in study design, experimental procedures, data analysis, manuscript preparation, or the decision to submit the manuscript.

Authors' contributions

SJH performed most of the experiments, analyzed the data, prepared the figures, and drafted the manuscript. MZX and HPF contributed substantially to the animal and cellular experiments and data analysis. WW, PSY and LKH participated in the experiments and data collection. ZY and DZL provides hUC-MSCs as well as related ethical and technical services. ZZB participated in the study design, data discussion, and manuscript revision. HCH conceived and supervised the study, acquired funding, and critically revised the manuscript. All authors read and approved the final manuscript.

Acknowledgements

The authors declare that they have not used AI-generated work in this manuscript.

The authors gratefully acknowledge Vcanbio Cell & Gene Engineering Corp., Ltd. for generously providing the human umbilical cord-derived mesenchymal stem cells (hUC-MSCs) used in this study.

References

1. Ma J, Chen Y, Si Y, Qian J, Wang C, Jin J, et al. The multifaceted nature of diabetic erectile dysfunction: un covering the intricate mechanisms and treatment strategies. Front Endocrinol (Lausanne). 2024;15:1460033.

2. Dilixiati D, Waili A, Tuerxunmaimaiti A, Tao L, Zebibula A, Rexiati M. Risk factors for erectile dysfunction in diabetes mellitus: a systematic review and meta-analysis. Front Endocrinol (Lausanne). 2024;15:1368079.

3. Zhang LW, Piao S, Choi MJ, Shin HY, Jin HR, Kim WJ, et al. Role of increased penile expression of transfo rming growth factor-beta1 and activation of the Smad signaling pathway in erectile dysfunction in streptozot ocin-induced diabetic rats. J Sex Med. 2008;5(10):2318-29.

4. Cabrini MR, Sezen SF, Lagoda G, Segal RL, Feng Z, Andreoni C, et al. Fibrotic protein expression profiles i n penile tissue of patients with erectile dysfunction. Urology. 2013;82(4):975.e1-6.

5. Ruan Y, Li M, Wang T, Yang J, Rao K, Wang S, et al. Taurine Supplementation Improves Erectile Function in Rats with Streptozotocin-induced Type 1 Diabetes via Amelioration of Penile Fibrosis and Endothelial Dy sfunction. J Sex Med. 2016;13(5):778-85.

6. Capogrosso P, Albersen M, Burnett AL, Cakir OO, Dehó F, Morgado LA, et al. Erectile Dysfunction: Update on Clinical Management. Eur Urol. 2025;88(4):388-99.

7. Patel AA, Shafie A, Mohamed AH, Ali SA, Tayeb FJ, Waggiallah HA, et al. The promise of mesenchymal st romal/stem cells in erectile dysfunction treatment: a review of current insights and future directions. Stem Ce ll Res Ther. 2025;16(1):98.

8. Li L, Li J, Guan H, Oishi H, Takahashi S, Zhang C. Human umbilical cord mesenchymal stem cells in diabet es mellitus and its complications: applications and research advances. Int J Med Sci. 2023;20(11):1492-507.

9. Feng H, Liu Q, Deng Z, Li H, Zhang H, Song J, et al. Human umbilical cord mesenchymal stem cells amelior ate erectile dysfunction in rats with diabetes mellitus through the attenuation of ferroptosis. Stem Cell Res Th er. 2022;13(1):450.

10. Shan Y, Zhang M, Tao E, Wang J, Wei N, Lu Y, et al. Pharmacokinetic characteristics of mesenchymal stem cells in translational challenges. Signal Transduct Target Ther. 2024;9(1):242.

11. Cecerska-Heryć E, Goszka M, Serwin N, Roszak M, Grygorcewicz B, Heryć R, et al. Applications of the reg enerative capacity of platelets in modern medicine. Cytokine Growth Factor Rev. 2022;64:84-94.

12. Masterson TA, Molina M, Ledesma B, Zucker I, Saltzman R, Ibrahim E, et al. Platelet-rich Plasma for the Tr eatment of Erectile Dysfunction: A Prospective, Randomized, Double-blind, Placebo-controlled Clinical Tria l. J Urol. 2023;210(1):154-61.

13. Greenberg DR, Panken EJ, Amarasekera C. Platelet-Rich Plasma for Urologic Conditions: An Early Call for Composition Reporting. J Urol. 2024;211(2):313-6.

14. Israeli JM, Lokeshwar SD, Efimenko IV, Masterson TA, Ramasamy R. The potential of platelet-rich plasma injections and stem cell therapy for penile rejuvenation. Int J Impot Res. 2022;34(4):375-82.

15. Wang K, Li Z, Li J, Liao W, Qin Y, Zhang N, et al. Optimization of the Platelet-Rich Plasma Concentration f or Mesenchymal Stem Cell Applications. Tissue Eng Part A. 2019;25(5-6):333-51.

16. Saraswathibhatla A, Indana D, Chaudhuri O. Cell-extracellular matrix mechanotransduction in 3D. Nat Rev Mol Cell Biol. 2023;24(7):495-516.

17. Raines EW, Bornfeldt KE. Integrin alpha(7)beta(1) COMPels smooth muscle cells to maintain their quiescen ce. Circ Res. 2010;106(3):427-9.

18. Da X, Li Z, Huang X, He Z, Yu Y, Tian T, et al. AGGF1 therapy inhibits thoracic aortic aneurysms by enhan cing integrin α7-mediated inhibition of TGF-β1 maturation and ERK1/2 signaling. Nat Commun. 2023;14(1) :2265.

19. Bonnans C, Chou J, Werb Z. Remodelling the extracellular matrix in development and disease. Nat Rev Mol Cell Biol. 2014;15(12):786-801.

20. Younesi FS, Miller AE, Barker TH, Rossi FMV, Hinz B. Fibroblast and myofibroblast activation in normal ti ssue repair and fibrosis. Nat Rev Mol Cell Biol. 2024;25(8):617-38.

21. Albersen M, Lin G, Fandel TM, Zhang H, Qiu X, Lin CS, et al. Functional, metabolic, and morphologic char acteristics of a novel rat model of type 2 diabetes-associated erectile dysfunction. Urology. 2011;78(2):476.e 1-8.

22. Dominici M, Le Blanc K, Mueller I, Slaper-Cortenbach I, Marini F, Krause D, et al. Minimal criteria for defi ning multipotent mesenchymal stromal cells. The International Society for Cellular Therapy position stateme nt. Cytotherapy. 2006;8(4):315-7.

23. Pan F, Zhang J, Liu Y, Lu L, Qiu X, Lv K, et al. Intracavernosal Pressure Recording to Evaluate Erectile Fun ction in Rodents. J Vis Exp. 2018(136).

24. Schneider CA, Rasband WS, Eliceiri KW. NIH Image to ImageJ: 25 years of image analysis. Nat Methods. 2012;9(7):671-5.

25. Cissell DD, Link JM, Hu JC, Athanasiou KA. A Modified Hydroxyproline Assay Based on Hydrochloric Acid in Ehrlich's Solution Accurately Measures Tissue Collagen Content. Tissue Eng Part C Methods. 2017;23(4):243-50.

26. Lou R, Shui W. Acquisition and Analysis of DIA-Based Proteomic Data: A Comprehensive Survey in 2023. Mol Cell Proteomics. 2024;23(2):100712.

27. Zhang Y, Yi D, Hong Q, Cao J, Geng X, Liu J, et al. Platelet-rich plasma-derived exosomes boost mesenchymal stem cells to promote peripheral nerve regeneration. J Control Release. 2024;367:265-82.

28. Jacob D, Hay J, Rahemtoola MS, Sim S, Libretto L, Chawareb EA, et al. Current advances in platelet-rich plasma therapy for erectile dysfunction: a meta-analysis of randomized controlled trials. J Sex Med. 2026;23(1).

29. Lee MJ, Kim SH, Shin S, Kim TW, Jo CH. Platelet-rich plasma enhances local homing of umbilical cord-derived mesenchymal stem cells to articular cartilage by increasing the quantity and activation of integrin β1. Stem Cell Res Ther. 2025;16(1):487.

30. Wang S, Zhang A, Liu K, Pan Y, Kang J, Niu S, et al. A study of diabetes-induced erectile dysfunction treated with human umbilical cord mesenchymal stem cells. Andrologia. 2022;54(7):e14440.

31. Liao CH, Lee KH, Chung SD, Chen KC, Praveen Rajneesh C, Chen BH, et al. Intracavernous Injection of Platelet-Rich Plasma Therapy Enhances Erectile Function and Decreases the Mortality Rate in Streptozotocin-Induced Diabetic Rats. Int J Mol Sci. 2022;23(6).

32. Sturny M, Anguenot L, Costa-Fraga FP, Bragina ME, Lima AM, da Silva RF, et al. Apelin-13 Protects Corpus Cavernosum Against Fibrosis Induced by High-Fat Diet in an MMP-Dependent Mechanism. J Sex Med. 2021;18(5):875-88.

33. Xia M, Yuan Y, Fang D, Tan X, Zhao F, Li X, et al. Blocking TSP1 Ameliorates Diabetes Mellitus-Induced Erectile Dysfunction by Inhibiting the TGF-β/SMAD Pathway. World J Mens Health. 2025;43(3):580-94.

34. Che D, Fang Z, Yan L, Du J, Li F, Xie J, et al. Elevated pigment epithelium-derived factor induces diabetic erectile dysfunction via interruption of the Akt/Hsp90β/eNOS complex. Diabetologia. 2020;63(9):1857-71.

35. Zhou B, Chen Y, Yuan H, Wang T, Feng J, Li M, et al. NOX1/4 Inhibitor GKT-137831 Improves Erectile Function in Diabetic Rats by ROS Reduction and Endothelial Nitric Oxide Synthase Reconstitution. J Sex Med. 2021;18(12):1970-83.

36. Yang W, Fang J, Zhai J, Qiu C, Liang Z, Liu Q, et al. IL-17A exacerbates corpus cavernosum fibrosis and neurogenic erectile dysfunction by inducing CSMC senescence via the mTORC2-ACACA pathway. BMC Med. 2024;22(1):376.

37. Bae SG, Yin GN, Ock J, Suh JK, Ryu JK, Park J. Single-cell transcriptome analysis of cavernous tissues reveals the key roles of pericytes in diabetic erectile dysfunction. Elife. 2024;12.

38. Yao C, Zhang X, Yu Z, Jing J, Sun C, Chen M. Effects of Stem Cell Therapy on Diabetic Mellitus Erectile Dysfunction: A Systematic Review and Meta-analysis. J Sex Med. 2022;19(1):21-36.

39. Margiana R, Pilehvar Y, Amalia FL, Lestari SW, Supardi S, I'Tishom R. Mesenchymal stem cell secretome: A promising therapeutic strategy for erectile dysfunction? Asian J Urol. 2024;11(3):391-405.

40. Ji YH, Zhang YF, Tan X, Hou HZ, Yao Z, Zhang B. High-activity placenta-derived mesenchymal stem cells combined with low-intensity extracorporeal shock wave therapy for diabetic erectile dysfunction: a prospective randomized controlled trial. Stem Cell Res Ther. 2025;16(1):359.

Supplementary Files

This is a list of supplementary files associated with this preprint. Click to download.

- SupplementaryMaterial.docx